Available online at www.sciencedirect.com
SCIENCE DIRECT
ELSEVIER
Journal of the European Ceramic Society 26 (2006) 2431–2440
ECERS
www.elsevier.com/locate/jeurceramsoc

Densification and properties of transition metal borides-based cermets via spark plasma sintering

T. Venkateswaran [a], B. Basu [a,*], G.B. Raju [a], Doh-Yeon Kim [b]

[a] *Laboratory for Advanced Ceramics, Department of Materials and Metallurgical Engineering, Indian Institute of Technology, Kanpur 208016, India*
[b] *School of Materials Science and Engineering and Center for Microstructure Science of Materials, Seoul National University, Seoul 151-744, Korea*

Received 20 December 2004; received in revised form 5 May 2005; accepted 15 May 2005
Available online 2 August 2005

Abstract

Engineering borides like TiB_2 and ZrB_2 are difficult to sinter materials due to strong covalent bonding, low self-diffusion coefficient and the presence of oxide layer on the powder particles. The present investigation reports the processing of hard, tough and electrically conductive transition metal borides (TiB_2 and ZrB_2) based cermets sintered with 6 wt.% Cu using spark plasma sintering (SPS) route. SPS experiments were carried out with a heating rate of 500 K/min in the temperature range of 1200–1500 °C for a varying holding time of 10–15 min and the optimization of the SPS conditions is established. A maximum density of ~95% ρ_{th} in ZrB_2/Cu and ~99% ρ_{th} in TiB_2/Cu is obtained after SPS processing at 1500 °C for 15 min. While the optimized TiB_2/Cu cermet exhibits hardness and fracture toughness of ~17 GPa and ~11 MPa $m^{1/2}$, respectively, the optimized ZrB_2/Cu cermet has higher hardness of ~19 GPa and fracture toughness of ~7.5 MPa $m^{1/2}$, respectively. High electrical conductivity of ~0.20 $M\Omega^{-1}$ cm^{-1} (TiB_2/Cu) and ~0.15 $M\Omega^{-1}$ cm^{-1} (ZrB_2/Cu) are also measured with the optimally sintered cermets.

Keywords: TiB_2; Sintering; Electron microscopy; Hardness; Toughness and toughening; Electrical conductivity; Spark plasma sintering

1. Introduction

Transition metal borides, an important class of advanced structural ceramic materials, are candidate materials for various applications, i.e. armor materials, aluminum evaporation boat, cathode material for hall-heroult cell, cutting tool, electro discharge machining (EDM) electrode, wear parts, high temperature applications, electrical devices, in rockets nozzles, in foundry or refractory applications, etc.[1–5] This is due to the fact that the borides like TiB_2 and ZrB_2 are characterized by high melting point (>3000 °C), high hardness (TiB_2: ~25–32 GPa, ZrB_2: ~22–25 GPa), elastic modulus (TiB_2: 510–575 GPa, ZrB_2: 440–460 GPa), wear resistance, good oxidation resistance, excellent thermal and electrical properties. Although having excellent properties, the borides have low to moderate fracture toughness (4–5 MPa $m^{1/2}$), primarily because of the inherent bonding nature. Furthermore, low self-diffusion coefficient and the presence of oxide layers (B_2O_3 and TiO_2 on TiB_2 particles, B_2O_3 on ZrB_2 particles) poses additional difficulties in the sintering of these TiB_2 and ZrB_2 transition borides.[1–5] Therefore, major research largely focused on using various sintering additives/binders to attain maximum densification and to improve the toughness of borides.

As far as the densification is concerned, considerable research activity is directed towards optimizing (a) processing parameters and (b) proper amount binder addition (metallic or ceramic binders). Hot pressing as well as dynamic compaction (DC) is reported to be quite effective in achieving maximum densification at lower temperature in the range of 1800 °C, while conventional pressureless sintering requires high temperature of ~2000 °C to obtain better densification, which is typically attained in the presence of binders.[6,7] Sintering additives play a major role in triggering sintering kinetics and thus helps in achieving maximum densification.

* Corresponding author. Tel.: +91 512 2597771; fax: +91 512 2597505.
E-mail address: bikram@iitk.ac.in (B. Basu).

0955-2219/$ – see front matter © 2005 Elsevier Ltd. All rights reserved.
doi:10.1016/j.jeurceramsoc.2005.05.011

Moreover, some sintering aids also improve specific properties, i.e. toughness, oxidation resistance, electrical properties, in addition to obtain better densification. Various metallic binders, investigated widely, are Ni, Cr, Fe, etc.[6,7] Cemented borides with a metallic binder have recently been developed in the TiB_2-Fe system. TiB_2-based cermets typically contain TiB_2 as a major phase, bonded with metallic phase (Co/Ni).[8] These materials are expected to be a novel lower density substitute for the WC/Co system. In recent times, $MoSi_2$ has also been used as sinter-additives in developing TiB_2-based high temperature materials. Both the hot processing as well as SPS processing parameters to obtain dense TiB_2–$MoSi_2$ ceramic composites are optimized and reported elsewhere.[9,10]

Another serious problem with high temperature sintering of ceramics like TiB_2 and ZrB_2 is the exaggerated grain growth, which in turn leads to the formation of micorcraks due to thermal anisotropy during cooling.[2,3] This leads to the degradation in mechanical properties (strength, hardness). To this end, faster sintering techniques like SPS can produce dense borides while restricting the grain growth and thereby enhancing mechanical properties, like hardness. The spark plasma sintering (SPS), a variant of activated sintering, is characterized by the application of electric current in addition to applied pressure. SPS process is reported to trigger superfast densification of nanomaterials without considerable grain growth.[10–13] In the present investigation, the densification study on the TiB_2 and ZrB_2 is conducted with the use of the metallic binder addition (Cu) in SPS route. The aim of the present investigation is to illustrate the influence of Cu binder on the densification behavior of two different borides in an electric field assisted sintering process. The optimization of SPS temperature to obtain maximum densification and better mechanical and electrical properties in TiB_2 and ZrB_2 is reported in the current work.

2. Experimental procedure

2.1. Starting powders and densification

Commercial TiB_2 and ZrB_2 were used as the major bulk phase in our composites. Both the boride powders are procured from Aldrich, USA and have average particle size <5 μm. The commercially available high purity copper (<5 μm, Aldrich, Korea) is used as a sintering aid for both TiB_2 and ZrB_2. During the preparation of cermets, TiB_2:Cu and ZrB_2:Cu in the weight ratio of 94:6 was mixed in a mixer for 24 h in 1 l of toluene in a polyethylene bottle. To break the agglomerates and to ensure better dispersion, WC balls were used during the mixing process, followed by drying in the oven.

The dried premixed powders are placed inside the graphite mold, ensured with proper insulation around the inside wall of the graphite mold (10 mm internal diameter) using thin graphite sheet to avoid contamination during sintering. The graphite punches are inserted into the mold and the graphite mold is placed between the graphite electrodes of SPS chamber. The SPS chamber is closed firmly and high vacuum of 70 mtorr is maintained throughout the experiment. During SPS experiments, DC current of 1–1.5 kA, DC voltage of 5–10 V and pulse frequency of 30–40 kHz are applied and variation in this range depends on the final holding temperature. The experiments are carried out in the temperature range of 1200–1500 °C with a heating rate of 500 K/min with the varying holding period of 10 and 15 min. A constant pressure of 40 MPa is maintained during the heating and holding period. The current flow is stopped and pressure is released as soon as the holding at sintering temperature is over. The final thickness of the sintered discs was about 2–3 mm.

2.2. Characterization

After complete removal of protective graphite insulating layer around the specimen, the density of spark plasma synthesized samples was measured in water following Archimedes principle. The theoretical densities of the corresponding composites were calculated by rule of mixture, taking density of TiB_2, ZrB_2 and Cu as 4.52, 6.06 and 8.9 g cm^{-3}, respectively. Further, phase identification was performed using X-ray diffraction using Cu Kα radiation (Rich-Seifert, 2000 D). The Vickers indentation is carried out on smoothly polished surface to measure hardness and toughness at indent load of 10 kg with a dwelling time of 15 s on a universal hardness tester. The fracture toughness is evaluated by measuring crack length measurement (2c) of the radial crack pattern formed around Vickers indents, adopting formulation proposed by Anstis et al.[14] The reported values are the average of five indentation tests. Detailed Microstructural investigation of the polished and fractured composites was performed using Scanning Electron Microscopy (FEI QUANTA SEM, Philips). Elemental compositional analysis of different phases are examined using EDS analysis and X-ray mapping on SEM. Room temperature electrical resistivity (dc) was measured by standard four probe method at room temperature with appropriate silver epoxy-coating on the flat materials, followed by hardening at 150 °C.

3. Results and discussion

3.1. Densification

At the first stage of the present work, the SPS experiments were carried out on TiB_2/Cu system and the SPS parameters were optimized. In the later experiments with ZrB_2/Cu, the SPS parameters were selected based on our experience in densifying TiB_2/Cu materials. The densification data of the TiB_2–6 wt.% Cu and ZrB_2–6 wt.% Cu cermets, Spark Plasma Sintered at various sintering temperature (1200–1500 °C) and various holding period (10 and 15 min) is presented in Fig. 1. Fig. 1a reveals the densification behavior of the TiB_2–6 wt.% Cu composites, indicating that the developed

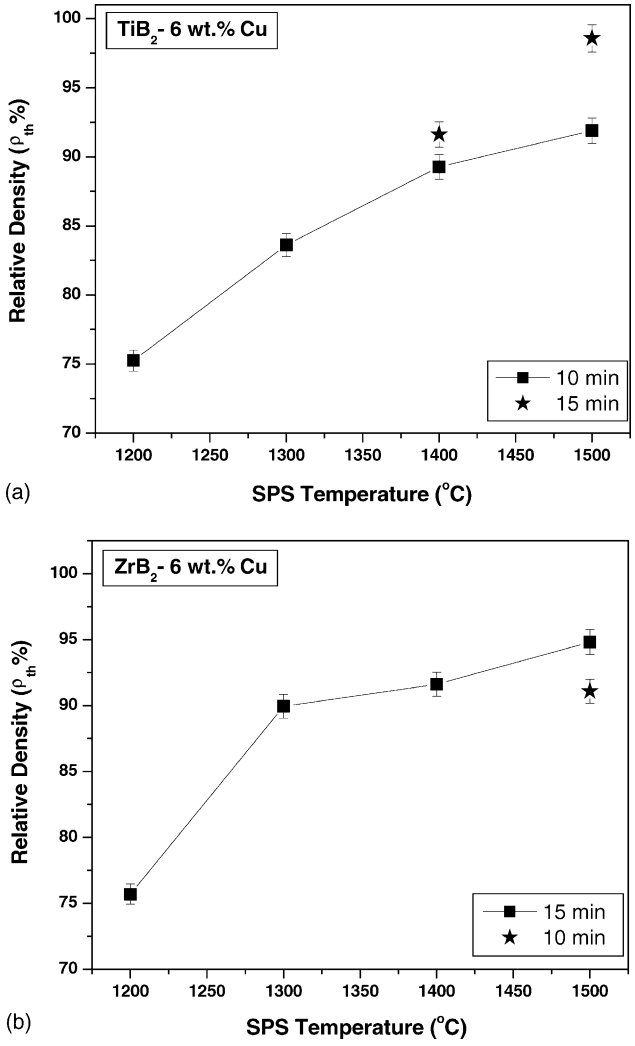

Fig. 1. Plot of relative density vs. SPS temperature spark plasma synthesized TiB_2–6 wt.% Cu (a) and ZrB_2–6 wt.% Cu (b) cermets for various holding time at peak sintering temperature.

TiB_2-based cermet with maximum density of ~99% ρ_{th} could be obtained after SPS processing at 1500 °C for a holding period of 15 min. Initially, the sintering was carried out for TiB_2/Cu cermets for the short holding period of 10 min for varying sintering temperature (1200–1500 °C) and the sintered density of more than 90% ρ_{th} was obtained only after SPS processing at 1500 °C. In general, the densification behavior exhibits a gradual increase in sintered density with increasing sintering temperature form 1200 to 1500 °C. Subsequently, the densification experiments were conducted with little longer holding period of 15 min at the sintering temperature of 1400 and 1500 °C in order to achieve higher densification. There is a considerable densification improvement with increasing the holding period from 10 to 15 min at 1500 °C. The difference in sintered density with holding time is however not significant at SPS temperature of 1400 °C.

In the light of the observed trend in densification of TiB_2/Cu cermet, the subsequent SPS experiments to obtain dense ZrB_2/Cu cermets were carried out for 15 min at varying temperatures between 1200 and 1500 °C. Fig. 1b shows the densification trend exhibited by ZrB_2–6 wt.% Cu cermet. The maximum densification of ~95% ρ_{th} is obtained, when SPSed at 1500 °C. Moreover, to ensure whether similarly high densification at shorter holding period of 10 min is feasible for the ZrB_2-based cermet, additional experiments were conducted at 1500 °C. The results reveals that both borides (TiB_2 and ZrB_2) with lower amount (6 wt.%) of sintering additives (Cu) exhibits maximum densification at sintering temperature of 1500 °C for a holding period of 15 min. When comparing the densification behavior of both the cermets, the TiB_2/Cu-based cermet exhibits almost theoretical density of ~99% ρ_{th}, when compared to ZrB_2/Cu cermet (~95% ρ_{th}) densified under identical SPS conditions (1500 °C, 15 min).

Our recent work showed that ~98% ρ_{th} can be obtained in monolithic TiB_2 after hot pressing at 1800 °C for 1 h.[9] As far as the processing of monolithic borides is concerned, TiB_2 is densified to 96.8% ρ_{th} after hot pressing at 1850 °C for 1 h.[27] However, much less sintered density of 87% ρ_{th} is obtained for monolithic ZrB_2 after hot pressing at 1900 °C for 0.5 h.[32] Hence, the present experimental results clearly indicate that both Cu addition as well as SPS processing enables to achieve faster densification at 1500 °C for 15 min with a heating rate of 500 K/min. To this end, it can also be mentioned that our previous investigation on the TiB_2-based material with ceramic binder ($MoSi_2$) addition, sintered via SPS route, revealed maximum densification (~98% ρ_{th}) at 1400 °C.[10] Collectively looking at densification behavior, the grain boundary cleaning effect contribution from SPS and liquid phase sintering (LPS) from Cu together contribute to achieve maximum densification at lower temperature in a shorter time. The LPS and physical activation due to electric field effect enhance the kinetics of the sintering and aid in mass transport effectively, which results in better densification.

From the phenomenological point of view, the liquid phase sintering involves the dissolution of ceramic phase in a sintering liquid followed by precipitation. The primary requirement therefore is that the liquid phase must wet the grain boundary of ceramic grains and also there should be an appreciable dissolution from ceramic phase in liquid phase at sintering temperature. Since both the cermets are processed under identical sintering conditions, the difference in sintering behavior should be attributed to the difference in dissolution of TiB_2 and ZrB_2 in Cu binder phase, which has a melting point of 1085 °C. Also, the wetting of individual TiB_2 or ZrB_2 phase by Cu melt could be different at the same SPS temperature (1500 °C). In order to study this, both Ti–Cu and Zr–Cu phase diagrams are considered.[33] From the Ti–Cu equilibrium diagram, it is clear that the solubility of Cu in Ti decreases with increase in temperature beyond melting point of Cu. For example, the maximum solubility of Cu at 1400 °C is 20 wt.%, which decreases to 12 wt.% at 1500 °C. Although Cu also dissolves in Zr, but to a lesser extent beyond melting of Cu. According to equilibrium Zr–Cu diagram, around 14 wt.% Cu at 1400 °C, and around 10 wt.% Cu at 1500 °C

can be dissolved in Zr. However, under fast heating rate and shorter sintering time, the dissolution could be less from the expected equilibrium level.

The densification result of the present study is further compared with that of earlier developed boride-based materials. Cheng and Gadalla processed the ZrB_2 cermets with higher amount of copper (25 vol.%) in the temperature range of 1100–1650 °C. The obtained materials exhibit poor sintered density (<80% ρ_{th}) due to evaporation of Cu and boron loss.[15] Densification of the TiB_2–(0.5 wt.%) Fe and Cr cermet was carried out in the temperature range of 1800–1900 °C for 2 h to obtain maximum densification (~98–99% ρ_{th}).[16] Ferber et al. have used upto 10 wt.% Ni to achieve more than 99% theoretical density in TiB_2 cermets by hot pressing route (~1400 °C).[17] It was reported by Einarsrud et al. that the effect of relatively small addition of (1–5 wt.%) of nickel, NiB and iron promotes the liquid phase sintering of TiB_2.[6] Mishra et al. sintered ZrB_2 with varying Fe and Cr content (5–20 wt.%) at sintering temperature of 1800 °C for 1 h. It was observed that the addition of Fe upto 10 wt.% enhances the densification (~93% ρ_{th}) and more addition of Fe decreases the sintered density. Additionally, Cr addition caused the swelling problem, leading to severe cracking.[7] From the above observations, it is clear that attaining high density (≥95% ρ_{th}) in boride-based cermets at lower temperature of 1500 °C via SPS route is a promising result.

3.2. Microstructure

The cermets selected for detailed microstructure study are the materials, which exhibit maximum in densification behavior (SPSed at 1500 °C, 15 min). XRD spectra obtained with the TiB_2–6 wt.% Cu and ZrB_2–6 wt.% Cu cermets are presented in Fig. 2. Fig. 2a shows the phase analysis of the TiB_2-based cermet, revealing the predominant presence of TiB_2 and metallic Cu. No reaction product is detected within the resolution limit of XRD. Similarly, Fig. 2b presents the XRD results of ZrB_2-based cermet, characterized by the presence of ZrB_2 as the main phase and Cu as the minor phase. There is no indication of formation of any reaction product. SEM micrographs (BSE contrast) of the polished and fractured surface of TiB_2–6 wt.% Cu cermet, SPSed at 1500 °C are displayed in Fig. 3. The microstructure of the TiB_2-based cermet is characterized by the presence of three phases with difference in electron contrast, i.e. black (pores), grey (Cu-rich phase) and dark (TiB_2). The fracture surface (Fig. 3c) of the TiB_2–6 wt.% Cu cermet is characterized by predominantly intergranular fracture mode. On the polished surfaces (Fig. 3b), the presence of pores having rounded as well as hexagonal morphology is observed in the TiB_2 grains. The TiB_2 grains in the cermet exhibits different morphology of faceted, rounded, platelet like (Fig. 3a). Moreover, the size of the TiB_2 grains is non-uniform in nature. The presence of coarser grains of size >5 μm can be noticed (Fig. 3a). The observation of finer as well as coarser/elongated grains with

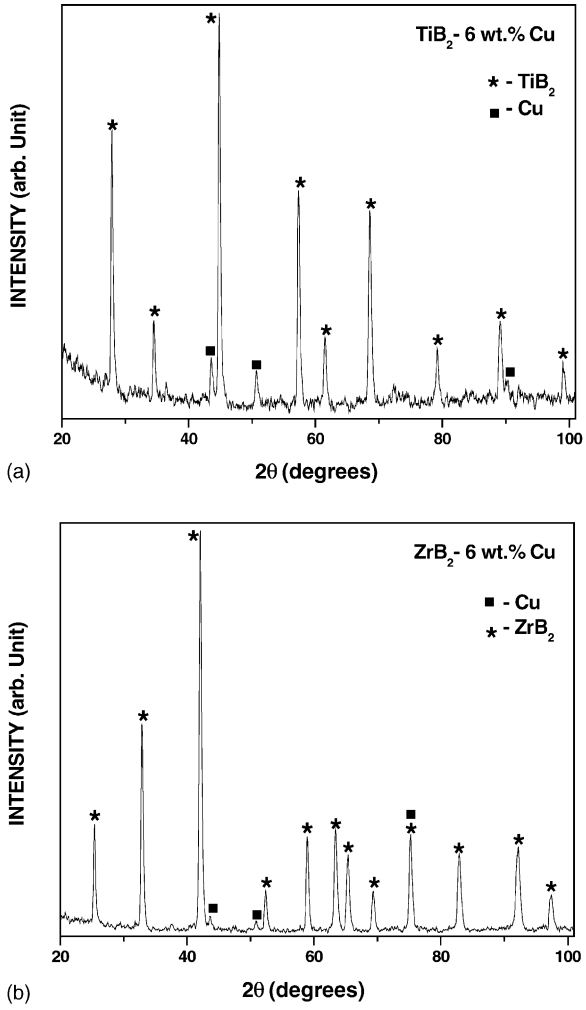

Fig. 2. X-ray diffraction spectra obtained with polished of TiB_2–6 wt.% Cu (a) and ZrB_2–6 wt.% Cu (b), SPSed at 1500 °C for 15 min under vacuum. The different crystalline phases are also indicated.

longer aspect ratio is also made. It is difficult to characterize the cermet with a characteristic grain size.

A closer look at the microstructure reveals the existence of a rim phase with dissolved Ti and Cu around the TiB_2 grains, as evident in Fig. 4. This dissolution of Cu presumably plays an important role in the shape change of the TiB_2 grains. It has been reported by Chae et al. that the irregular solid grain is formed due to the dissolution and reprecipitation at certain specific grain surfaces.[18] This type of grain shape change can be correlated with the tendency towards attaining the equilibrium grain shape or to obtain more stable structure. Han et al. observed the shape change from faceted to spherical ZnO grains in the presence of the Bi_2O_3 liquid.[19] In the present case, an observation of shape change at higher temperature (1400–1500 °C) is predominantly observed with the cermet sintered for longer holding time of 15 min. Based on the above observations, it can be stated that Ti from borides dissolve in the liquid Cu phase and reprecipitation of (Ti, Cu) solid solution takes place on TiB_2 particles during SPS process. The dissolution–precipitation

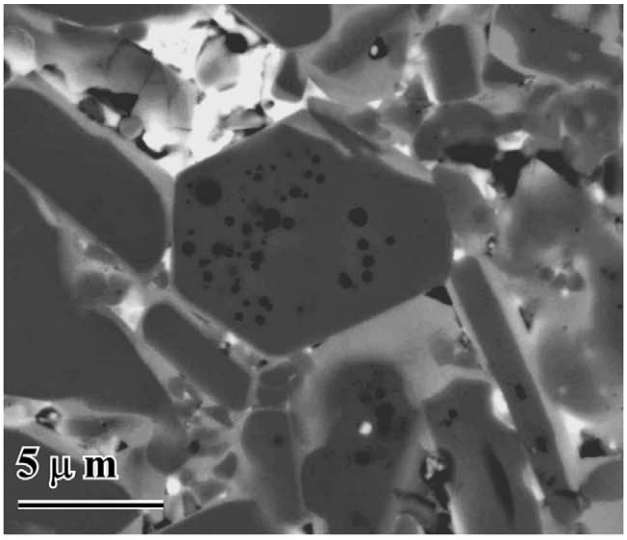

(a)

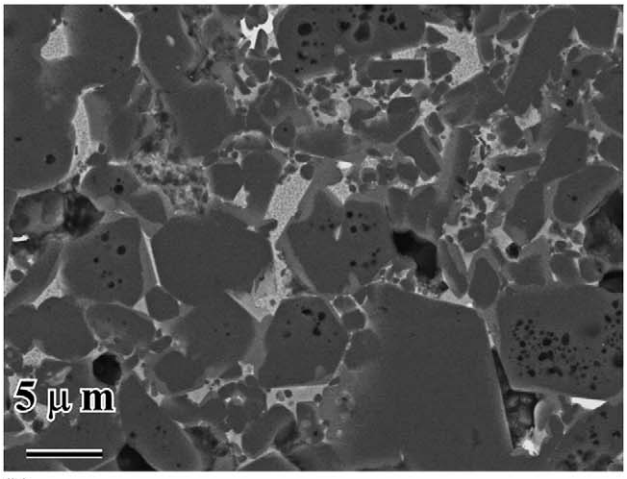

(b)

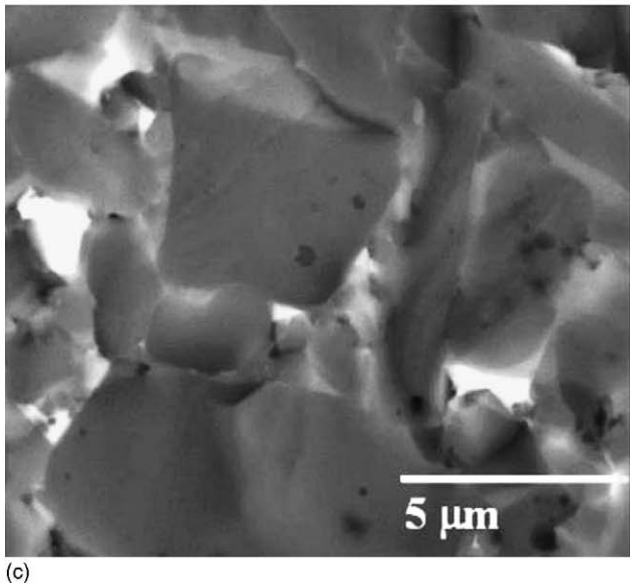

(c)

Fig. 3. Scanning electron micrographs of polished surface (a, b) and fracture surface (c) exhibiting different morphology (rounded, elongated, plate like) of TiB_2 grains (grey contrast) the TiB_2–6 wt.% Cu composite, SPSed at 1500 °C for 15 m under vacuum. The presence of pores within boride grains can be noted.

process, being dependent on starting particle shape and size, occurs with varying extent in our TiB_2/Cu cermets.

The X-ray mapping analysis is carried out on the selected region of polished TiB_2–6 wt.% Cu cermets. Fig. 4 shows the corresponding microstructural region along with X-ray intensity distribution of relevant elements (Ti, B, Cu). The X-ray mapping results indicate the predominant presence of Ti and B (black phase), constituent elements of the titanium di-boride. The presence of Cu is much clear around the TiB_2 grains and appears as a gray phase. The presence of Cu ensures proper wetting of the TiB_2 grains. EDS analysis of the white or bright contrast phase indicate the presence of W, which may incur during the initial ball milling experiments. Overall, the presence of Cu (melting point ∼1085 °C and boiling point ∼2595 °C) helps in the densification of the cermet at much lower temperature.

Fig. 5 illustrates SEM images of the polished and fracture surface of the ZrB_2–6 wt.% Cu cermet, SPSed at 1500 °C for 15 m under vacuum. Observing the fracture surfaces (Fig. 5b), it is apparent that the fracture takes place by mixed mode of transgranular and intergranular type. Similar to TiB_2 cermets, the observation of three different phases like ZrB_2 particles, Cu-rich phase and a third phase with different electrons contrast of grey, white, black, respectively, can be made in the polished cross section (Fig. 5a). The presence of a large amount of entrapped porosity within the ZrB_2 grains and in the metallic Cu rich phase, correlates well with the lower densification (∼95% ρ_{th}). X-ray mapping of the ZrB_2–6 wt.% Cu cermet is also carried out on selected regions of a smoothly polished sample (Fig. 6). X-ray mapping reveals the predominant presence of Zr and B, constituent elements of the ZrB_2 phase (black phase). There is significant observation of Cu surrounding the ZrB_2 grains and predominantly along the triplet junctions. The presence of W is detected by EDS analysis of white contrast phase, similar to that in the case of the TiB_2 cermet. Compared to TiB_2 cermet, the variation in grain size as well as shape is not large in ZrB_2 cermets. The presence of a characteristic core-rim structure, with a rim phase having different electron contrast, can be critically made. SEM–EDS analysis indicated that while core phase is predominantly ZrB_2, the rim phase has reduced Zr content with dissolved Cu. Also, the comparison of Figs. 3 and 5 reveals that the dissolution–precipitation occurs to a lesser extent in ZrB_2-based cermet as compared to TiB_2 cermet. Similar core-rim structure is widely reported for various ceramic materials like Y-TZP[20] as well as cermet materials like TiCN–Ni[21], etc.

3.3. Mechanical and electrical properties

Tables 1 and 2 present the mechanical properties of the developed TiB_2 and ZrB_2 cermets, SPSed at 1500 °C for a holding period of 15 m under vacuum. The TiB_2–6 wt.% Cu exhibits optimum hardness and fracture toughness of ∼17 GPa and ∼11 MPa $m^{1/2}$, respectively. The fracture toughness of the cermet is almost double than that of the monolithic TiB_2 (∼5 MPa $m^{1/2}$), hot pressed at 1850 °C

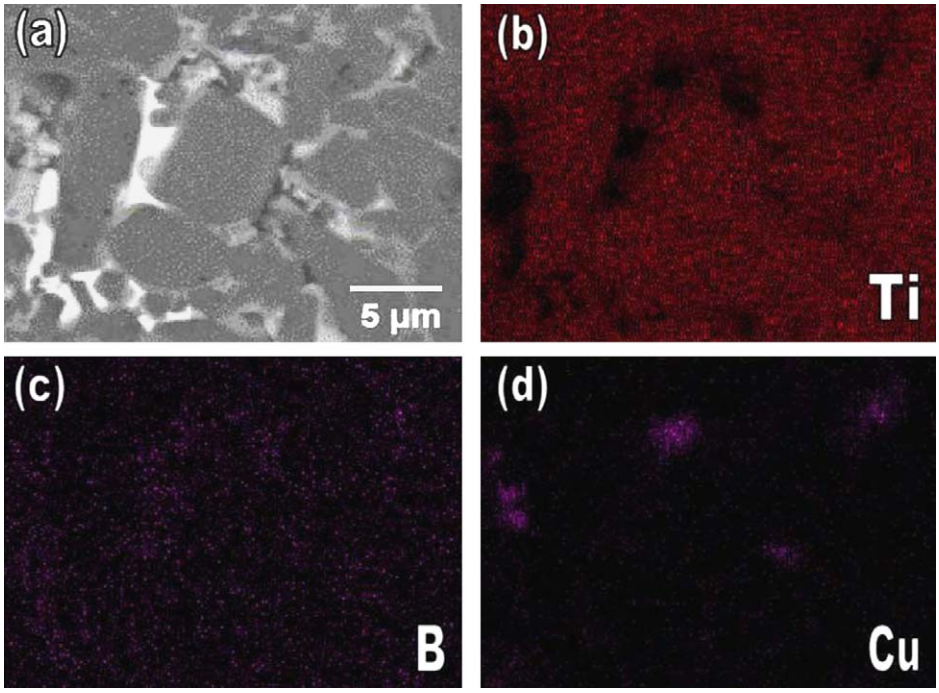

Fig. 4. X-ray mapping analysis of the TiB_2–6 wt.% Cu composite, SPSed at 1500 °C for 15 min in vacuum. X-ray intensity maps for relevant elements; Ti (b), B(c) and Cu (d) as well as the investigated microstructural region are shown (a) (polished section).

for 1 h.[27] It can also be noted that the TiB_2-based cermet with 0.5 wt.% Fe and Cr addition, pressureless sintered at 1800 °C exhibits strength of 506 MPa and fracture toughness of 6.6 MPa $m^{1/2}$, respectively.[16] TiB_2 with 1.4 wt.% Ni, hot pressed at 1400 °C exhibits strength and fracture toughness of 670 MPa and 6.4 MPa $m^{1/2}$, respectively. Addition of Ni more than 2 wt.% to TiB_2 results in the formation of brittle grain boundary phase, which in turn degrades the properties.[17] Comparing the data presented in Table 1, it is clear that the fracture toughness of the newly developed TiB_2 cermets is much higher than earlier developed cermets, whereas the hardness is lower. The difference in mechanical properties should be attributed to the difference in the TiB_2 grain size and dissolution of TiB_2 during sintering. Certainly, the TiB_2

Table 1
A table comparing the density, hardness, fracture toughness and electrical conductivity of the SPSed TiB_2 and TiB_2–6 wt.% Cu cermet materials with various TiB_2-based cermets and monolithic TiB_2, developed earlier

Material	Processing details	Relative density (% ρ_{th})	Vickers hardness (H_V) (GPa)	Indentation toughness (K_{IC}) (MPa $m^{1/2}$)	Electrical resistivity (ρ, μΩ cm)	Electrical conductivity (ρ, $M\Omega^{-1}$ cm^{-1})	Reference
Monolithic TiB_2	PS, 2100 °C, 1 h, vacuum	99.3	–	4.8	8.4	0.119	26
Monolithic TiB_2	HP, 1850 °C, 1 h, vacuum	96.8	24.4	5.4	14.0	0.071	27
TiB_2–0.7 wt.% Ni	HP, 1550 °C, 1 h, vacuum	97.9	23.3	5.1	9.0	0.111	27
TiB_2–1.4 wt.% Ni	HP, 1425 °C	>99	–	6.4	–	–	17
TiB_2–7.9 wt.% Ni	HP, 1425 °C	>99	–	4.0	–	–	17
TiB_2–0.5 wt.% Fe–0.5 wt.% Cr	PS, 1800 °C, 2 h, argon	97.6	27.0	6.2	–	–	16
TiB_2–19.8 wt.% Fe–8.6 wt.% Ni	HIP, 1350 °C, argon	–	13.9	5.5	–	–	30
TiB_2–40 wt.% Cu	SHS + HIP, >2000 °C, 12 h	96.1	–	8.3	–	–	28
TiB_2–33 wt.% Co	HIP, 1350 °C, 1/2 h, argon	–	17.0	2.9	–	–	29
TiB_2–6.0 wt.% Cu	SPS, 1500 °C, 15 min	98.6	16.7	10.9	4.9	0.204	Present work

Different processing routes are indicated: PS, pressureless sintering; HP, hot pressing; HIP, hot isostatic pressing; SHS, self-propagating high temperature synthesis and SPS, spark plasma sintering.

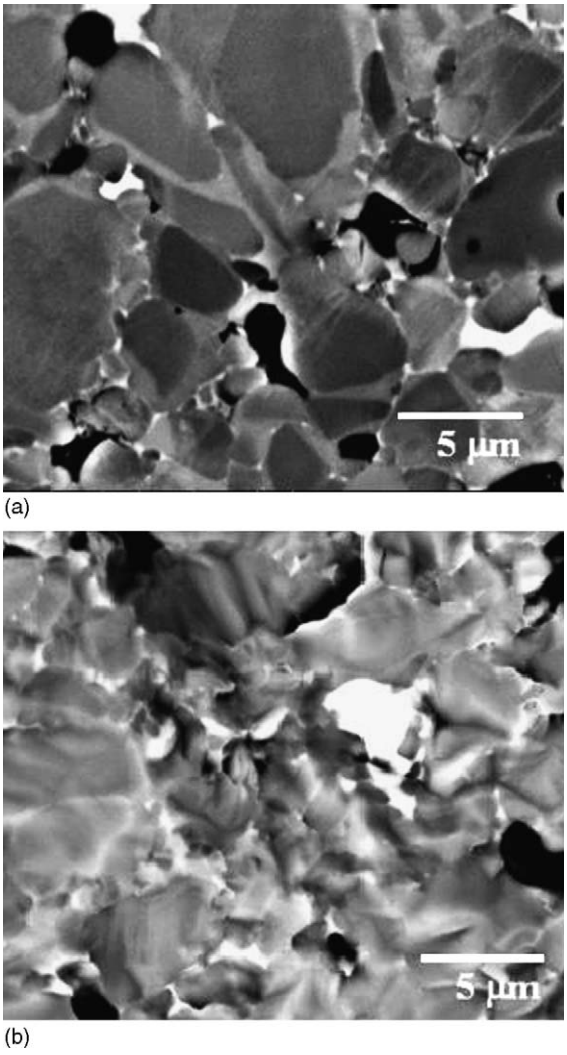

Fig. 5. Scanning electron micrographs of polished surface showing varying grain size of ZrB_2 particles (grey contrast) and presence of rounded pores trapped in between the grains and there is an observation of diffusion of secondary phase Cu along the boundaries of the Zr matrix phase (a) and fracture surface of the ZrB_2–6 wt.% Cu composite exhibiting transgranular type (b) of the composite SPSed at 1500 °C for a holding period of 15 m under vacuum.

grains in our cermet exhibit a wider grain size distribution with considerable number of grains having sizes of >5 μm, which restrict the hardness. In case of the pressureless sintering as well as the pressure assisted sintering processes, high temperature and longer holding time presumably leads to grain growth as well as the extensive solid solution formation by dissolution of TiB_2, which in turn detracts the hardness of the materials. In case of SPS process, its effect is minimal. In our experiments, the addition of softer phase like Cu upto 6 wt.% does not seem to considerably degrade the hardness as hardness of 17 GPa is measured in SPS processed TiB_2–6 wt.% Cu cermet.

The optimally densified ZrB_2–6 wt.% Cu exhibits higher hardness and fracture toughness of ∼19 GPa and ∼7.5 MPa $m^{1/2}$, respectively. Table 2 illustrates the comparison of material properties of the newly developed cermet with the earlier developed ZrB_2-based materials. ZrB_2–4 wt.% Ni, hot pressed at 1850 °C for 30 min exhibits high hardness and very low fracture toughness of 14.4 GPa and 3.4 MPa $m^{1/2}$, respectively.[22] On the other hand, ZrB_2 sintered with 13 wt.% B_4C is reported to have higher hardness and fracture toughness of 19.2 GPa and 4.5 MPa $m^{1/2}$, respectively.[22] Zhang et al. synthesized ZrB_2–SiC composite via reactive hot pressing at 1900 °C with an applied pressure of 30 MPa under argon atmosphere for 60 min. The bending strength and fracture toughness of the developed composite reported to be 506 MPa and 4 MPa $m^{1/2}$, respectively.[23] Therefore, a comparison with literature results, as mentioned above, suggests that ZrB_2–6 wt.% Cu has higher hardness than earlier developed ZrB_2–Ni cermet. More importantly, the fracture toughness of ZrB_2/Cu cermet is much higher than earlier developed ZrB_2 materials, as reported elsewhere.[22,23]

The attainment of higher toughness in the newly developed cermets needs to be critically noted. In the case of monolithic TiB_2, the contribution to toughness arises primarily from crack deflection. Whereas in case of cermets, the ductile metal bridging contributed significantly by crack closure in enhancing the fracture toughness. When a crack propagates in boride cermets, the crack gets deflected by the coarser boride particles. Also, the metallic binder phase

Table 2
The density, hardness and fracture toughness and electrical resistivity of the SPSed ZrB_2–6 wt.% Cu cermet material

Material	Processing details	Relative density (% ρ_{th})	Vickers hardness (H_V) (GPa)	Indentation toughness (K_{IC}) (MPa $m^{1/2}$)	Electrical resistivity (ρ, μΩ cm)	Electrical conductivity (ρ, $M\Omega^{-1}$ cm^{-1})	Reference
ZrB_2	HP 1900 °C, 0.5 h	86.5	8.7	3.5	–	–	31
ZrB_2–4 wt.% Ni	HP 1850 °C, 0.5 h	98.0	14.4	2.8	–	–	31
ZrB_2	HP 1900 °C, 0.5 h, vacuum	87.0	8.7	2.35	15	0.066	32
ZrB_2–4 wt.% Ni	HP 1850 °C, 0.5 h	98.0	14.4	2.8	7.42	0.134	22
55 wt.% ZrB_2–41 wt.% TiB_2–4 wt.% Ni	HP 1600 °C, 0.5 h	∼100	17.7	4.3	15.55	0.064	22
83 wt.% ZrB_2–13 wt.% B_4C–4 wt.% Ni	HP 1870 °C, 10 min	99.6	19.2	4.5	16.08	0.062	22
ZrB_2–6 wt.% Cu	SPS 1500 °C, 15 min	94.8	19.1	7.4	6.5	0.133	Present work

For comparison, the literature data are also mentioned. Different processing routes are indicated: HP, hot pressing and SPS, spark plasma sintering.

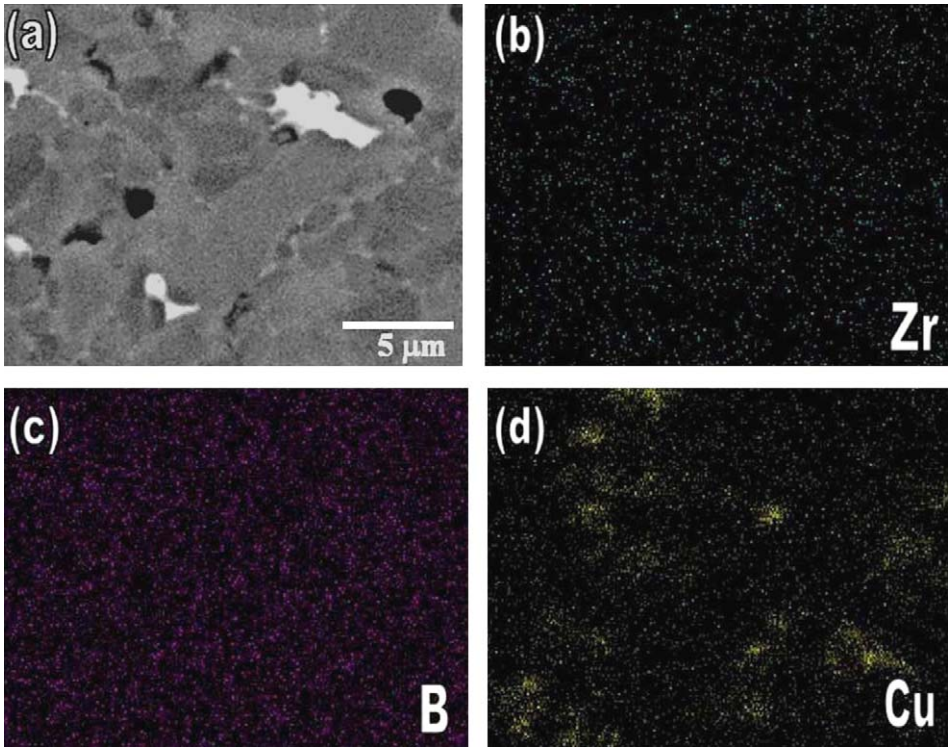

Fig. 6. X-ray mapping analysis of the Spark Plasma Sintered (1500 °C, 15 min) ZrB_2–6 wt.% Cu cermet, exhibits the predominant presence of base constituent elements Zr (b) and B (c) and Cu binder phase around ZrB_2 grains (d). The analyzed microstructural region (polished surface) is shown in (a).

(Cu) plastically flows around the crack tip of a propagating crack. Both these factors contribute together to achieve higher toughness in the newly developed cermets. It can be mentioned here that similar mechanism also contributes to enhanced toughness (∼13–14 MPa $m^{1/2}$) of WC–6 wt.% Co cermets.[24]

Apart from the mechanical properties, the electrical resistivity of the optimized cermets is measured at room temperature using conventional four probe method. The developed materials, i.e. TiB_2- and ZrB_2-based cermets exhibit low resisitivity of ∼5 and 6.5 μΩ cm, respectively, and high electrical conductivity of 0.20 and 0.15 $M\Omega^{-1}$ cm^{-1}, respectively. The higher resistivity of ZrB_2 cermets is presumably due to higher entrapped porosity. The TiB_2-based materials exhibit better conductivity than ZrB_2-based composite material, because of better interconnected network of metallic binder phase. It can be noted here that the electrical resistivity of pure TiB_2 is 10–30 μΩ cm and that of pure ZrB_2 is 9.2 μΩ cm. The electrical resisitivity of the Cu–48 vol.% TiB_2 composite, developed by Yin and Chung, is reported to be ∼3.4 μΩ cm.[25] The electrical resisitivity of the recently developed TiB_2 and TiB_2–10 wt.% $MoSi_2$ composite exhibits in the range of 13.2 μΩ cm and 12.5 μΩ cm, respectively.[10] From the above discussion, it should be evident that the addition of smaller amount of Cu, in the present case, significantly increases the electrical properties of the borides.

Comparing the material properties of our cermets with the earlier developed cermets, it is to be noted that the earlier cermets were primarily processed via pressureless sintering or hot pressing or hot isostatic pressing (see Tables 1 and 2). In case of earlier developed TiB_2-based cermets, hardness of more than 20 GPa is measured with a maximum of ∼27 GPa with TiB_2–0.5% Fe–0.5% Cr cermet (Table 1). Although, the hardness of the SPSed cermet is lower (17 GPa), but the fracture toughness is much higher (∼11 MPa $m^{1/2}$), in fact two to three times higher than that of earlier developed cermets (∼3–6 MPa $m^{1/2}$). Also, the SPSed cermets have much better electrical conductivity (∼0.2 $M\Omega^{-1}$ cm^{-1}), which is twice than that of either monolithic TiB_2 or TiB_2–0.7% Ni (see Table 1).

Similar observation, with little exception, is also made for ZrB_2-based cermets. The hardness of the SPSed cermet is comparable or even better than that of the earlier developed ZrB_2 materials (Table 2). As far as the toughness is concerned, the indentation toughness of the SPSed cermet (7.4 MPa $m^{1/2}$) is much higher than that of other ZrB_2-based materials, which varies in the range 2.4–4.5 MPa $m^{1/2}$. The electrical conductivity of SPSed cermet is comparable with the hot pressed ZrB_2–4% Ni cermet (∼0.134 $M\Omega^{-1}$ cm^{-1}) and even much better than other ZrB_2-based materials, as reported in Table 2.

As a concluding note, the fabrication of transition metal borides-based cermets, as reported in the present work, resembles an important class of cermets, i.e. WC-Co hardmetal, which combines the high toughness and electrical conductivity of a metallic binder with the hardness of the boride phase. The microstructure of the obtained

cermets are similar to that of other cermet materials like Ti(CN)–Ni.[21] The present experimental results also reveal that the combination of better mechanical properties, in particular high toughness, and electrical properties can be achieved in TiB_2 and ZrB_2-based cermet. The developed cermets can be used as a candidate material for various engineering applications, especially as electro discharge machining electrodes. Because of good combination of moderate hardness and high toughness, these cermets can also be potentially used as wear parts and cutting tool inserts.

4. Conclusions

(a) In the present work, the influence of 6 wt.% Cu addition on the densification of two borides, e.g. TiB_2 and ZrB_2 is studied using SPS as a processing tool. Both the cermets were optimally densified to ~99% ρ_{th} (TiB_2–6 wt.% Cu) and 95% ρ_{th} (ZrB_2–6 wt.% Cu) at SPS temperature of 1500 °C with holding time of 15 min. The enhanced sintering at lower temperature is attributed to the liquid phase sintering and the electric field effect, inherent in SPS processing.

(b) The sintered microstructure is characterized by a core-rim structure with the dissolution of Ti/Zr in Cu melt and thereby forming a rim phase. Another characteristic microstructural feature is the change of grain shape of ceramic phase (TiB_2 or ZrB_2) from equiaxed to more rounded shape, which presumably is due to the dissolution–reprecipitation phenomenon inherent in liquid phase sintering.

(c) The mechanical property measurements revealed that the newly developed boride cermets are superior in terms of toughness, as compared to earlier developed cermets based on borides. While the optimum TiB_2 cermet exhibits high hardness and fracture toughness of 17 GPa and 11 MPa $m^{1/2}$, respectively; the ZrB_2 cermets has higher hardness of 19 GPa, but lower fracture toughness of ~7.5 MPa $m^{1/2}$.

(d) SPS processed cermets also exhibit better electrical conductivity property. The addition of 6 wt.% Cu leads to enhanced electrical conductivity in both TiB_2-based cermets (0.20 $M\Omega^{-1}$ cm^{-1}) as well as in ZrB_2-based cermets (0.15 $M\Omega^{-1}$ cm^{-1}). The higher resistivity or less conductivity in ZrB_2 cermet is particularly ascribed to the presence of more entrapped porosity.

Acknowledgement

Venkateswaran wishes to express sincere gratitude to the members of Sintering and Microstructure laboratory and thin film & Microstructure laboratory (TFML) for their help during SPS experiments.

References

1. Tennery, V. J., Finch, C. B., Yust, C. S. and Clark, G. W., Structure-property correlations for TiB_2-based ceramics Densified using active liquid metals. In *Science of Hard Materials*, ed. Viswanadhan *et al.* Plenum, New York, 1983, pp. 891–909.
2. Wilkins, J. M. L., In *Boron and Refractory Borides*, ed. V. I. Matkovich. Spring-Verlag, New York, 1977, p. 633.
3. Mroz, C., Titanium diboride. *Am. Ceram. Soc. Bull.*, 1995, **74**, 158–159.
4. Mortz, C., Zirconium diboride. *J. Am. Ceram. Soc. Bull.*, 1994, **73**(6), 141–142.
5. Sakai, K., Some characteristics and applications of ZrB_2 composite ceramics. *Ceram. Jpn.*, 1989, **24**, 526–532.
6. Einarsrud, M., Hagen, E., Petterson, G. and Grande, T., Pressureless sintering of titanium diboride with nickel, nickel boribe and iron additives. *J. Am. Ceram. Soc.*, 1997, **80**(12), 3013–3020.
7. Mishra, S. K., Das, S. K., Ray, A. J. and Ramachandrarao, P., Effect of Fe and Cr addition on the sintering behaviour of ZrB_2 produced by self-propagation high-temperature synthesis. *J. Am. Ceram. Soc.*, 2003, **85**(11), 2846–2848.
8. Sigl, L. S. and Schwetz, K. A., *Powder Metall. Int.*, 1991, **23**, 221.
9. Ch. Murthy, T. S. R., Basu, B., Balasubramaniam, R., Suri, A. K., Subramonian, C. and Fotedar, R. K., Processing and properties of novel TiB_2-based composites, *J. Am. Ceram. Soc.*, 2005 (in press).
10. Venkateswaran, T., Basu, B. and Kim, D.-Y., Spark plasma sintering of TiB_2-based composites, *J. Am. Ceram. Soc.*, submitted for publication.
11. Groza, J. R. and Zavalianges, A., Sintering activation by external electric field. *Mater. Sci. Eng.*, 2000, **A287**, 171–177.
12. Wang, S. W., Chen, L. D. and Hirai, T., Densification of Al_2O_3 powder using spark plasma sintering. *J. Mater. Res.*, 2000, **15**(4), 982.
13. Basu, B., Lee, J. H. and Kim, D. Y., Development of nanocrystalline wear resistant Y-TZP ceramics. *J. Am. Ceram. Soc.*, 2004, **87**(9), 1771–1774.
14. Anstis, G. R., Chantukul, P., Lawn, B. R. and Marshall, D. B., A critical evaluation of indentation techniques for measuring fracture toughness. *J. Am. Ceram. Soc.*, 1981, **64**, 553–557.
15. Cheng, Y. M. and Gadalla, A. M., Synthesis and analysis of ZrB_2-based composites. *Mater. Manuf. Process.*, 1996, **11**(4), 574–587.
16. Kang, S., Kim, D. J., Kang, E. S. and Baek, S. S., Pressureless sintering and properties of titanium diboride ceramics containing chromium and iron. *J. Am. Ceram. Soc.*, 2001, **84**(4), 893–895.
17. Ferber, M. K., Becher, P. F. and Finch C. B., In *Effect of Microstructure on the Properties of TiB2 Ceramics*, Communications of the American Ceramic Society, January 1983, pp. C2–C3.
18. Chae, K. W., Chun, D. I. and Kim, D. Y., Microstructural evolution during the infiltration treatment of titanium carbide–iron composite. *J. Am. Ceram. Soc.*, 1990, **73**(7), 1979–1982.
19. Han, J.-H., Chung, Y.-K., Kim, D.-H., Cho, S.-H. and Yoon, D. K., Temperature dependence of the shape of ZnO grains in a liquid matrix. *Acta. Metall.*, 1989, **37**(10), 2705–2708.
20. Kim, J. J., Park, C. and Kim, D. Y., Discontinuous coarsening of tetragonal precipitates in partially stabilized zirconia induced by diffusional coherency strain under applied stress. *J. Am. Ceram. Soc.*, 1990, **73**(12), 3658–3662.
21. Sarkar, D., Ahn, S., Kang, S. and Basu, B., Fretting wear of TiCN–Ni cermet: influence of secondary carbide content. *P/M Sci. Technol. Briefs*, 2003, **5**(2), 5–11.
22. Monteverde, F., Bellosi, A. and Guicciardi, S., Processing and properties of zirconium diboride-based composites. *J. Eur. Ceram. Soc.*, 2002, **22**, 279–288.

23. Zhang, G. Y., Deng, Z. Y., Kondo, N., Yang, J. F. and Ohji, T., Reactive hot processing of ZrB_2–SiC composites. *J. Am. Ceram. Soc.*, 2000, **83**(9), 2330–2332.
24. Basu, B., Lee, J.-H. and Kim, D.-Y., Development of WC-ZrO_2 nanocomposites by spark plasma sintering. *J. Am. Ceram. Soc.*, 2004, **87**(2), 317–319.
25. Yin, P. and Chung, D. D. L., Titanium diboride copper-matrix composite. *J. Mater. Sci.*, 1997, **32**, 1703–1709.
26. Baumgartner, H. R. and Steiger, R. A., Sintering and properties of TiB_2 made from powder synthesized in a plasma—Arc heater. *J. Am. Ceram. Soc.*, 1984, **67**(3), 207–212.
27. Bellosi, A. and Monteverde, F., Microstructure and properties of titanium nitride and titanium diboride-based composites, Euro PM99 properties, pp. 261–268.
28. Xu, Q., Zhang, X., Han, J., He, X. and Kvanin, V. L., Combustión síntesis and densification of titanium diboride-copper matrix composites. *Mater. Lett.*, 2003, **57**, 4439–4444.
29. Gonzalez, R., Barandika, M. G., Ona, D., Sanchez, J. M., Villellas, A., Valea, A. *et al.*, New binder phases for the consolidation of TiB_2 hardmetals. *Mater. Sci. Eng.*, 1996, **A216**, 185–192.
30. Sanchez, J. M., Barandika, M. G., Sevillano, J. G. and Castro, F., Consolidation, microstructure and mechanical properties of newly developed TiB_2-based materials. *Scripta Met. et Mater.*, 1992, **26**, 957–962.
31. Melendez-Martinez, J. J., Domínguez-Rodriguez, A., Monteverde, F., Melandri, C. and Portu, G. D., Characterization and high temperature mechanical properties of zirconium boride-based materials. *J. Eur. Ceram. Soc.*, 2002, **22**, 2543–2549.
32. Monteverde, F., Guicciardi, S. and Bellosi, A., Avances in microstructure and mechanical properties zirconium diboride based ceramics. *Mater. Sci. Eng. A*, 2003, **346**, 310–319.
33. Murray, J. L., Arias, D. and Abriata, J. P., *Alloy Phase Diagrams*, *Vol 3*. ASM Handbook, 1992.